A numerical model to assess the creep of shotcrete linings

A numerical model to assess the creep for shotcrete linings

Pierpaolo Oreste, PhD,[1], Giovanni Spagnoli, PhD, MBA[2], Luigi Alberto Ceravolo, MSc[3]

[1] Full Professor, Department of Environmental, Land and Infrastructural Engineering, Politecnico di Torino, Corso Duca Degli Abruzzi 24, 10129 Torino, Italy, ORCID: 0000-0001-8227-9807

[2] Global Project and Technology Manager Underground Construction, BASF Construction Solutions GmbH, Dr.-Albert-Frank-Straße 32, 83308 Trostberg, Germany, *giovanni.spagnoli@basf.com*; (corresponding author), ORCID: 0000-0002-1866-4345

[3] Research Fellow, Department of Environmental, Land and Infrastructural Engineering, Politecnico di Torino, Corso Duca Degli Abruzzi 24, 10129 Torino, Italy

Abstract

In this paper, the behavior of the sprayed concrete (SC) linings in the tunnel was analyzed considering the secondary deformation effects over time. Considering the behavior of SC support under the loads applied by the rock mass and the interaction between the lining and the rock mass, a detailed analysis of the stress and deformation was performed by using the Convergence Confinement the Hyperstatic Reaction Methods. In order to develop a procedure to perform a correct design of a shotcrete lining an analysis was required combined with the Convergence Confinement Method (CCM) and Hyperstatic Reaction Method (HRM). To take into account the creep phenomenon, the Voigt-Kelvin model was used for modelling the shotcrete, which employs two springs and a viscous damper to physically reproduce the actual behavior. Some useful considerations were obtained on the trend of the safety factors of the shotcrete linings over time.

KEY WORDS: Tunnels & tunnelling; Stress Analysis; Excavation; Mathematical modelling

Notation list

p_0: lithostatic pressure;

p_{cr}: critical pressure;

φ_p: peak friction angle of the rock mass;

c_p: peak cohesion of the rock mass;

R: tunnel radius;

R_{pl}: plastic radius;

c_r: residual cohesion of the rock mass;

φ_r: residual friction angle of the rock mass;

E_{rm}: elastic modulus of the rock mass;

v: Poisson coefficient of the rock mass;

E_i: elastic modulus of shotcrete at ith-step;

t_{sc}: thickness of the shotcrete lining;

v_{sc} : Poisson coefficient of the shotcrete;

ε_t: total deformation;

σ: applied load;

E_∞: elastic modulus of the shotcrete at infinity, when creep ceased;

E_1: initial elastic modulus of the shotcrete at $t = 0$;

E_2: elastic modulus of the shotcrete in the parallel creep scheme;

η: viscosity of the shotcrete;

Ψ: dilatancy.

Introduction

Neville et al. (1983) define creep as the increase in strain with time under a sustained stress, i.e. the material deforms not only due to the stresses which it is subjected to, but also due over a time during which these stresses are applied. Normally creep strain are not fully recovered, thus it is largely plastic deformation (Dusseault and Fordham, 1993). Goodman (1980) explains the creep as a viscous behavior. There are certain situations where strains increase with time. This is the case of tunnels excavated in very soft rock or heavily fractured rock under significant in-situ stresses (Yu, 1998; Dusseault and Fordham, 1993), in rocks of argillaceous nature (Barla, 2011), rock salts (Goodman,1980; Moghadam et al., 2013) or also due to the combination of the applied stress and material properties (exceeding a limiting shear stress), the geological conditions, the in situ stress conditions and the groundwater flow (Barla, 2001). For rocks containing clay, the phenomenon associated with water migration (or clay platelets orientation) could be considered as a type of consolidation (Goodman, 1980). However, the time-dependent behavior of rocks is normally not considered during tunnel design.

Creep phenomenon in sprayed concrete

Creep behavior is also very important in sprayed (or shot)concrete, SC (Thomas, 2009). For SC the principle of rheological models is the same as for rock (Thomas, 2009). Because SC linings are loaded at a very early age, the influence of time dependent material properties on the deformation behavior and bearing capacity is much more significant than in regular concrete structures (Schädlich and Schweiger, 2014). Regarding creep of SC, movement of water from the adsorbed layers on the cement paste to internal void may be the cause of creep (Thomas, 2009) and this theory is supported by the fact that creep increases with increasing porosity (Neville, 1995).

Numerical models are massively employed to assess the creep behavior of SC linings (e.g. Yin, 1996; Schröpfer, 1995; Schädlich and Schweiger, 2014), such as rheological models (Jaeger and Cook, 1979), Kelvin model (Neville et al., 1983; Jaeger and Cook, 1979; Rokahr

and Lux, 1987), Burgers model (Yin, 1996), viscoplastic model (Thomas, 2009). However, real creep behavior of linings is hard to understand as the load-bearing mechanism is a composite consisting of the ground and the lining behavior. The current simplistic approach to model SC linings in numerical simulations considers a linear elastic material with a step-wise increase of the Young's modulus in subsequent excavation stages. While realistic lining deformations may be obtained with this method, lining stresses are usually too high, in particular if the lining is subjected to significant bending (Schädlich and Schweiger, 2014).

According to (Huber, 1991, Neville et al., 1993, Thomas, 2009) creep of SC increases with humidity, cement content, increasing stress and decreasing strength. (Thomas, 2009) observed also that by increasing the proportion of aggregates the magnitude of creep is reduced. Besides, the paste is also responsible for the creep. As a matter of fact, aggregate undergoes very little creep. However, the aggregate influences the creep of concrete through a restraining effect on the magnitude of creep. The paste which is creeping under load is restrained by aggregate which do not creep.

Cement on the other hand does not have an influence on the creep behavior; however creep increases with an increase in water/cement ratio (Akroyd, 1962). Concrete reinforcement (e.g. fibers) reduces creep phenomenon, presumably due to the restraining effect (Ding, 1998).

Creep is significantly higher at an early stage of load as the strength of SC is lower, as found by (Huber, 1991) who observed that a sample loaded at 8 days creeps by 25% more than a similar sample loaded at 28 days. However, it must be kept in mind that some accelerators increase the early strengths (Melbye, 1994) therefore creep after 24 or 48 h is close to that at greater ages (Kuwajima, 1999). The stronger the aggregate the more is the restraining effect and hence the less is the magnitude of creep. However, synthetic fibers reinforced SC have twice the creep capacity than steel fibers reinforced SC (Thomas, 2009; MacKay and Trottier, 2004).

The numerical model

To study the behavior of the SC lining during the creep phases, a specific model has been developed. The method is based on the joint application of the CCM and HRM. With the CCM (Oreste, 2009; 2015; Spagnoli et al., 2016; 2017) it is possible to evaluate the initial load on the SC lining, through the intersection of the convergence-confinement curve (CCC) with the reaction line of the lining (see Fig. 1). To define the reaction line the initial elastic modulus of the SC (E_1) is considered, before the creep starts. Once the initial load is evaluated, it is possible to obtain by means of the HRM the exact path of the stress inside the lining at the initial condition. HRM investigates the behavior of SC lining under the loads applied by the rock mass and considering the interaction between the lining and the rock mass (Oreste, 2007, Do et al., 2014). The HRM models half of a tunnel section by beam elements connected by nodes. The elements develop bending moments, axial forces and shear forces. The interaction between ground and support is represented by “Winkler” type springs in the normal and tangential direction for each node of the model (Oreste et al., 2018).

The initial condition represents the situation at the end of the excavation and loading phases of the SC lining. Once the lining has been installed and is in full and effective contact with the ground, the support starts to deform as shown in Fig. 1. CCC qualitatively reflects the stress redistribution of the ground around the opening (Deere et al., 1970). The y-axis of Fig. 1 represents the load that must be applied to the walls of the opening to prevent any further deformation, whilst the x-axis is the tunnel wall convergence. OA represents the deformation occurring before the lining is installed. OB represents the deformation of the tunnel walls. AB is the deformation of the lining and BB' is the load in the support.

From this moment the analysis of the creep phenomenon starts, which evolve over the time. With the evolution of creep, SC shows a lower stiffness which implies an increase of the deformation in the lining. Therefore, the displacement of the tunnel wall increases. The deformation due to the creep (i.e. secondary deformation), causes a decrease of the applied loads

126 at the lining leading to a great benefit as this can avoid overloading (Thomas, 2009). The
127 specific model allows to consider two aspects:

128 • Higher deformation of the SC lining over time;
129 • Reduction of the loads on the lining due to the deformation and increase of the tunnel
130 wall displacement;

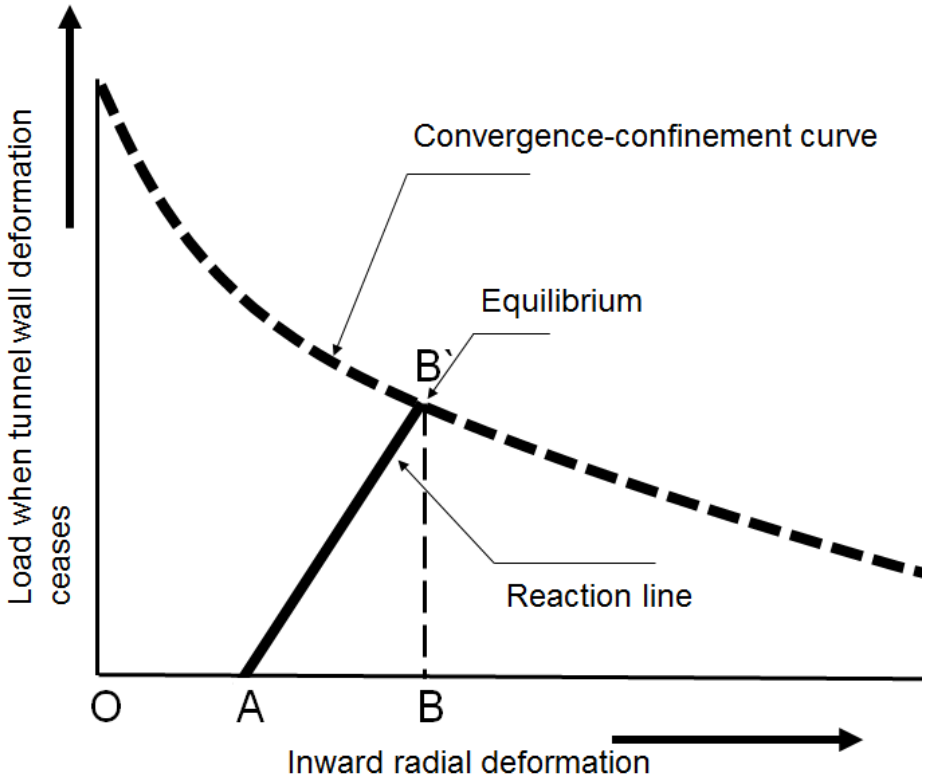

131

132 Fig. 1 Simplified load-deformation diagram at the end of the excavation and loading phase of
133 the SC lining. Keys: OA represents the deformation occurring before the lining is installed.
134 OB represents the deformation of the walls of the tunnel; AB represents the deformation of
135 the lining; BB' represents the load in the support.

136 In order to determine the stress and strain evolution of the lining over time (i.e. during the
137 creep), it is important to define the apparent elastic modulus of the SC lining at the infinity E_∞,
138 i.e. at the end of the creep. This value permits to draw a reaction line of the lining at the infini-
139 ty, and therefore, to obtain the final load acting on the lining (i.e. lower than the initial load)

from the intersection of the new reaction line with CCC. The stiffness k of the circular lining is function of the elastic modulus of the SC and therefore (Fig. 2):

$$k_{in} = \frac{R^2-(R-t_{sc})^2}{(1+v_{sc})\cdot[(1-2\cdot v_{sc})\cdot R^2+(R-t_{sc})^2]} \cdot \frac{1}{R} \cdot E_1 \quad (1)$$

$$k_{fin} = \frac{R^2-(R-t_{sc})^2}{(1+v_{sc})\cdot[(1-2\cdot v_{sc})\cdot R^2+(R-t_{sc})^2]} \cdot \frac{1}{R} \cdot E_\infty \quad (2)$$

where:

t_{sc} is the shotcrete lining thickness;

v_{sc} is the Poisson coefficient of the SC;

E_1 is the initial elastic modulus of the SC;

E_∞ is the elastic modulus of the shotcrete at infinity, i.e. the creep ceased;

k_{in} is the initial stiffness of the SC lining;

k_{fin} is the final stiffness of the SC lining;

R is the tunnel radius.

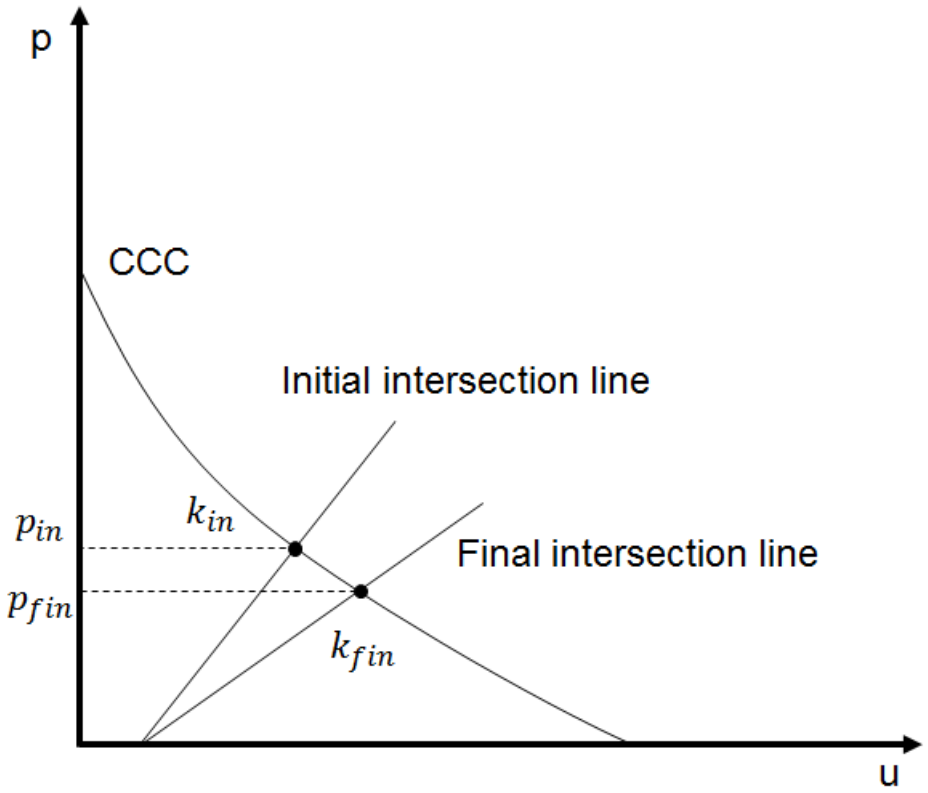

Fig. 2 Evaluation of the initial and final load on the lining through the convergence-confinement method. Key: *p* internal pressure of the tunnel; *u* radial displacement of the tunnel wall; k_{in} and k_{fin} initial and final stifness of the SC lining; p_{in} and p_{fin} initial and final load on the SC lining; CCC convergence-confinment curve.

The stress-strain analysis of the lining from the initial ($t = 0$) to the final condition $t = \infty$) is performed, through different calculation steps, with the HRM. Each step considers the application of a negative load Δp on the lining ($\Delta p=(p_{fin}-p_{in})/n$, where n is the step number) connected to a particular value of the elastic modulus of the SC. The results of each calculation steps, in terms of stress and strains in the SC, add to the situation resulting at the end of the previous step. Knowing the value Δp, it is possible to graphically obtain the mean path of the reaction line at each step (i) and the stiffness k_i. As the elastic modulus of the SC and the stiffness of the lining are depending on each other, it is possible to obtain the mean elastic modules E_i at each step:

$$E_i = \frac{k_i \cdot (1+v_{sc}) \cdot [(1-2 \cdot v_{sc}) \cdot R^2 + (R-t_{sc})^2] \cdot R}{R^2 - (R-s_{sc})^2} \quad (3)$$

For the determination of the time associated with the reduction of the elastic modulus of the SC corresponding to each step, the viscosity η comes into play. To take into account the effect of the viscosity due to the creep phenomenon, the Voigt-Kelvin model, consisting of two springs and a viscous damper, was used (see Fig. 3). Among the creep-models, the Voigt-Kelvin model is one of the three most commonly used rheological models, along with Maxwell model and the Burgers model, for SC linings (Thomas, 2009). It exhibits an exponential strain creep, i.e. it predicts very good creep and it assumes an uniform distribution of strain. The material is modelled with a viscous-elastic response. It consists of a spring in series with a parallel of another spring and a viscous damper.

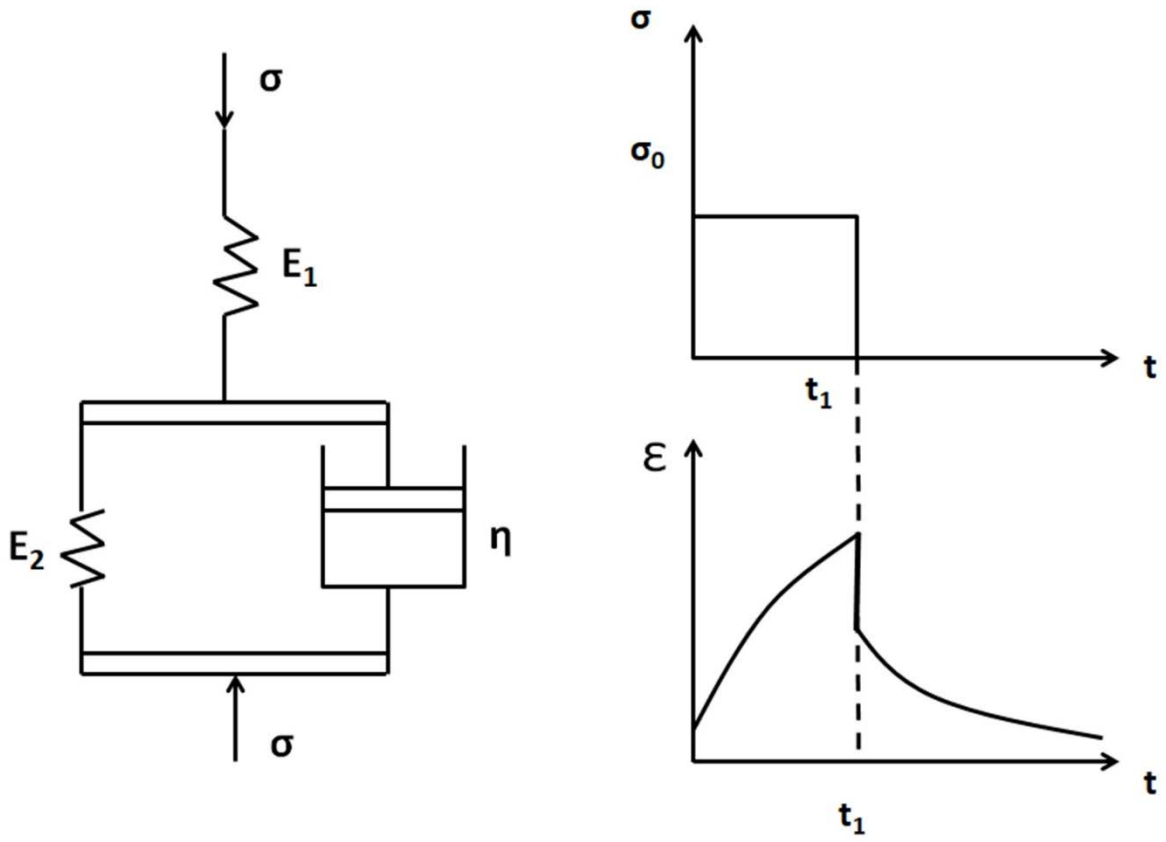

Fig. 3 Voigt-Kelvin creep model (σ is the applied load, E is the elastic modulus and η is the viscosity coefficient, ε is the deformation.

Gradual recovery of elastic deformation occurs. The total deformation will be:

$$\varepsilon_t = \frac{\sigma}{E_2} \cdot (1 - e^{-\frac{E_2 \cdot t}{\eta}}) + \frac{\sigma}{E_1} \quad (4)$$

where:

ε_t is the deformation over time;

σ is the applied load;

E is the elastic modulus;

In this case two different configurations have been adopted regarding secondary deformation.

- $\varepsilon_2 = \frac{1}{2}\frac{\sigma}{E_2}$ after t=3 years (ε_2, secondary deformation due to the parallel. After 3 years is half of the total secondary deformation);
- $\varepsilon_2 = \frac{1}{3}\frac{\sigma}{E_2}$ after t=3 years (ε_2, secondary deformation due to the parallel. After 3 years is one-third of the total secondary deformation).

The law of the Voigt-Kelvin model is as follows:

$$\varepsilon_t = \frac{\sigma}{E_2} \cdot (1 - e^{-\frac{E_2 \cdot t}{\eta}}) + \frac{\sigma}{E_1} \quad (5)$$

E_2 is obtained as:

$$\frac{1}{E_\infty} = \frac{1}{E_1} + \frac{1}{E_2} \quad (6)$$

Therefore:

$$E_2 = \frac{E_1 \cdot E_\infty}{E_1 - E_\infty} \quad (7)$$

Considering:

$$\varepsilon_2 = \frac{\sigma}{E_2} \cdot (1 - e^{-\frac{E_2 \cdot t}{\eta}}) \quad (8)$$

From the two different assumptions, i.e. ε_2 half and one-third of the total secondary deformation, the viscosity value, η, can be obtained. For example, considering the case in which it

is assumed that the ε_2 reaches half of the total value (at infinity) after a time t = 3 years, it will be:

$$\varepsilon_{2_{(t=3)}} = \frac{1}{2}\frac{\sigma}{E_2} = \frac{\sigma}{E_2} \cdot (1 - e^{-\frac{E_2 \cdot t}{\eta}}) \quad (9)$$

therefore:

$$e^{-\frac{E_2 \cdot 3}{\eta}} = \frac{1}{2} \quad (10)$$

The viscosity, η, will be:

$$\eta = \frac{-3 \cdot E_2}{\ln(\frac{1}{2})} \quad (11)$$

For the model the value of the elastic modulus will be:

$$E_t = \frac{1}{\frac{1}{E_1} + \frac{(1 - e^{-\frac{E_2 \cdot t}{\eta}})}{E_2}} \quad (12)$$

therefore:

$$t = \frac{-\eta \cdot \ln[\left(\frac{E_2}{E_1}\right) + 1 - \left(\frac{E_2}{E_t}\right)]}{E_2} \quad (13)$$

The time associated with the decrease of the elastic modulus corresponding to the midpoint of each of the 10 steps is thus obtained. With the proposed method it will be possible to conduct studies in terms of variations of normal and shear forces, rotation and bending moments. It is also possible to evaluate the decreases of the SC elastic modulus in each of the 10 calculation steps and the times associated to each step.

Numerical example

In the following examples, the calculation procedure previously explained was performed, in order to verify creep effects on the static conditions over time of the SC lining. 10 calculation steps (n=10) were considered in order to describe the stress and strain state in the creep phase. Each of the 10 calculation steps considers a decrease of the applied load Δp. For

each of them, a reaction line of the SC lining was obtained and from it the elastic modulus E_i and the corrisponding time.

Five cases were considered to calculate the creep in SC linings. Cases 1, 2, 4 and 5 refer to a rock with RMR = 30, whereas case 3 is for RMR = 60. These values were arbitrary selected to have a broader range of rock types. For case 1, $E_\infty = 75\%\, E_1$, assumed with a secondary deformation after 3 years being one-half of the total deformation. The viscosity was calculated as per equation 18. For case 2, $E_\infty = 50\%\, E_1$ however the secondary deformation is the same as for case 1. In case 3, E_∞ and the viscosity were the same as per case 1, however the rock was assumed to have better characteristics. In case 4, E_∞ is the same as per case 1 and case 3, however viscosity was calculated as per equation 16 (i.e. secondary deformation after 3 years being one-third of the total deformation). Finally, in case 5, E_∞ is the same as per case 2 but the secondary deformation is the same as per case 4.

Case 1

For the first four cases the rock mass properties are shown in Tab. 1.

Rock parameter	**Unity of measure**	**Value**
Elastic modulus (E_{rm})	[MPa]	3160
Coefficient of Poisson (v)	[-]	0.30
Peak cohesion (c_p)	[MPa]	0.15
Residual cohesion (c_r)	[MPa]	0.12
Peak friction angle (φ_p)	[°]	20
Residual friction angle (φ_r)	[°]	16

Dilatancy (ψ)	[°]	16

Tab. 1 Geomechanical parameters arbitrary assumed for the rock with RMR=30.

For the construction of the characteristic curve and of the reaction lines of the initial and final support (Fig. 4), the following assumptions were considered:

- the elastic module of the concrete $E_1 = 8000\ MPa$;
- the elastic modulus of the concrete at infinity, E_∞, for which in this first case a value equal to $E_\infty = 75\%\ E_1$ was adopted.

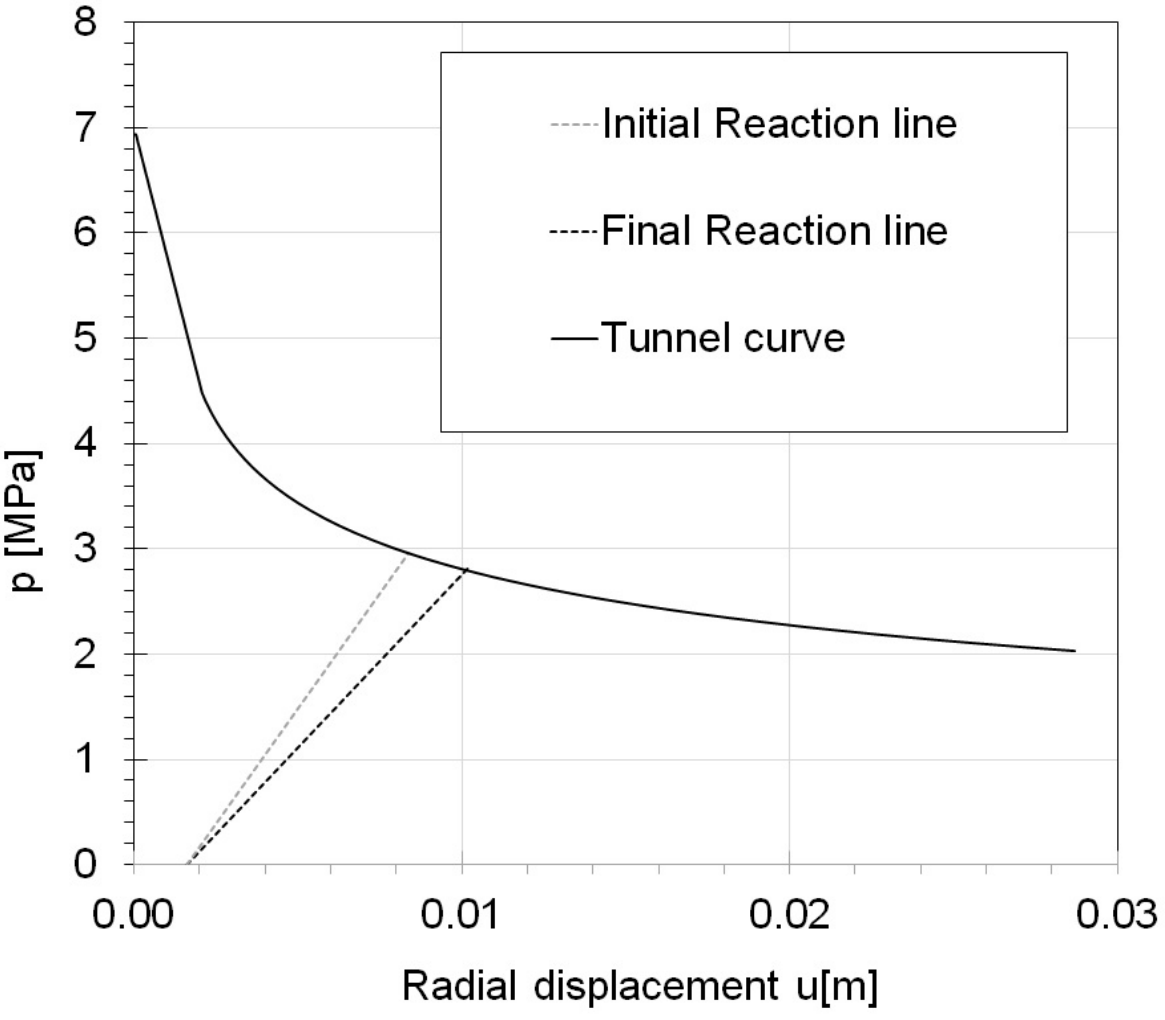

Fig. 4 Case 1: Convergence-confinement curve of the tunnel and the initial and final reaction line of the shotcrete lining.

The characteristic curve thus obtained shows displacements in the order of centimeters. Considering equations 6 and 7, we obtain:

$$E_{\infty} = \frac{3}{4} \cdot E_1 \tag{14}$$

Therefore, $E_2 = 3 \cdot E_1 = 24000\ MPa$.

To take into account the viscosity, it was assumed that after 3 years the secondary deformation is equal to one-third of the total deformation, and we will obtain:

$$\eta = \frac{-3 \cdot E_2}{\ln(\frac{1}{2})}\ \text{[MPa/year]} \tag{15}$$

Results are obtained using described procedure with the hyperstatic reaction method, in terms of variations from the initial condition (when the tunnel is completed, t=0), with black color, to the final condition (step i=10, t=∞), with grey color, for rotation, bending moments, shear and normal forces along the tunnel profile inside the shotcrete lining (see Fig. 5). For reasons of simplicity, only half of the covering is shown, starting from the center of the invert up to the center of the cap crown.

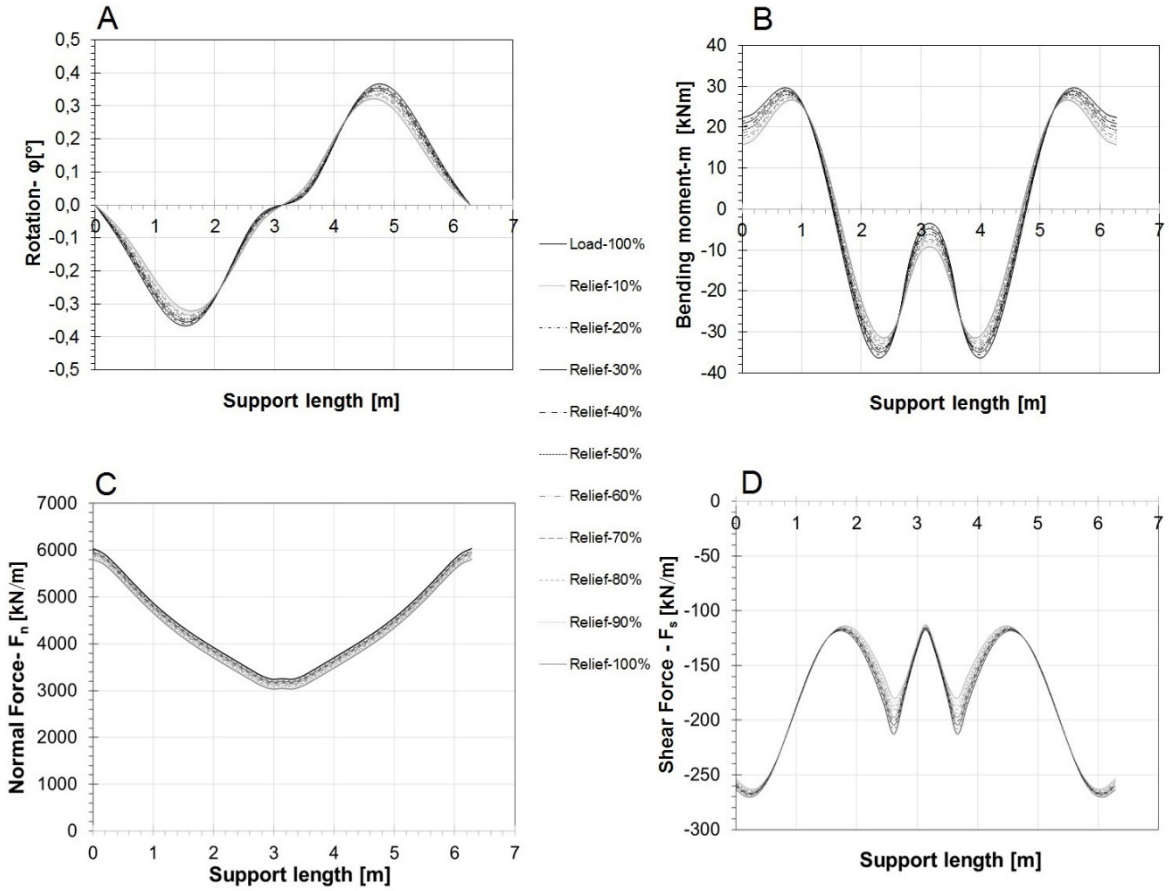

Fig. 5 Case 1: Results of rotation (A), bending moments (B), normal (C) and shear forces (D) for case 1 along the lining profile.

From case 1 it is possible to observe:

- Rotation tends to fade over time due to creep as well as bending moments that reduce more than normal forces. The resulting reductions, in terms of maximum in absolute value, are the following:
  - rotation: 12.33%;
  - bending moments: 14.82%;
  - normal forces: 3.83%;
  - shear forces: 2.88%.

As regards the variations of the elastic modulus corresponding to each step and the respective associated times, the results reported in Tab. 2 have been obtained.

Step	E shotcrete [MPa]	t [year]
1	7934.03	0.11
2	7763.18	0.42
3	7555.00	0.84
4	7347.53	1.34
5	7140.76	1.94
6	6934.70	2.67
7	6729.35	3.62
8	6524.72	4.91
9	6320.80	6.90
10	6117.59	11.10

Tab. 2 – Case 1: variation of the elastic modulus of the SC over time during the creep process, according to the adopted mechanical scheme; time associated to each step, after the construction phase (initial condition).

Case 2

In case 2, a different hypothesis was made regarding the value of E_∞. It was assumed $E_\infty = 50\% E_1$. The characteristic curve and the reaction lines of the lining will be different (Fig. 6). The displacements will be slightly higher than for case 1 and the difference between the initial and final reaction lines will be more evident with respect to case 1.

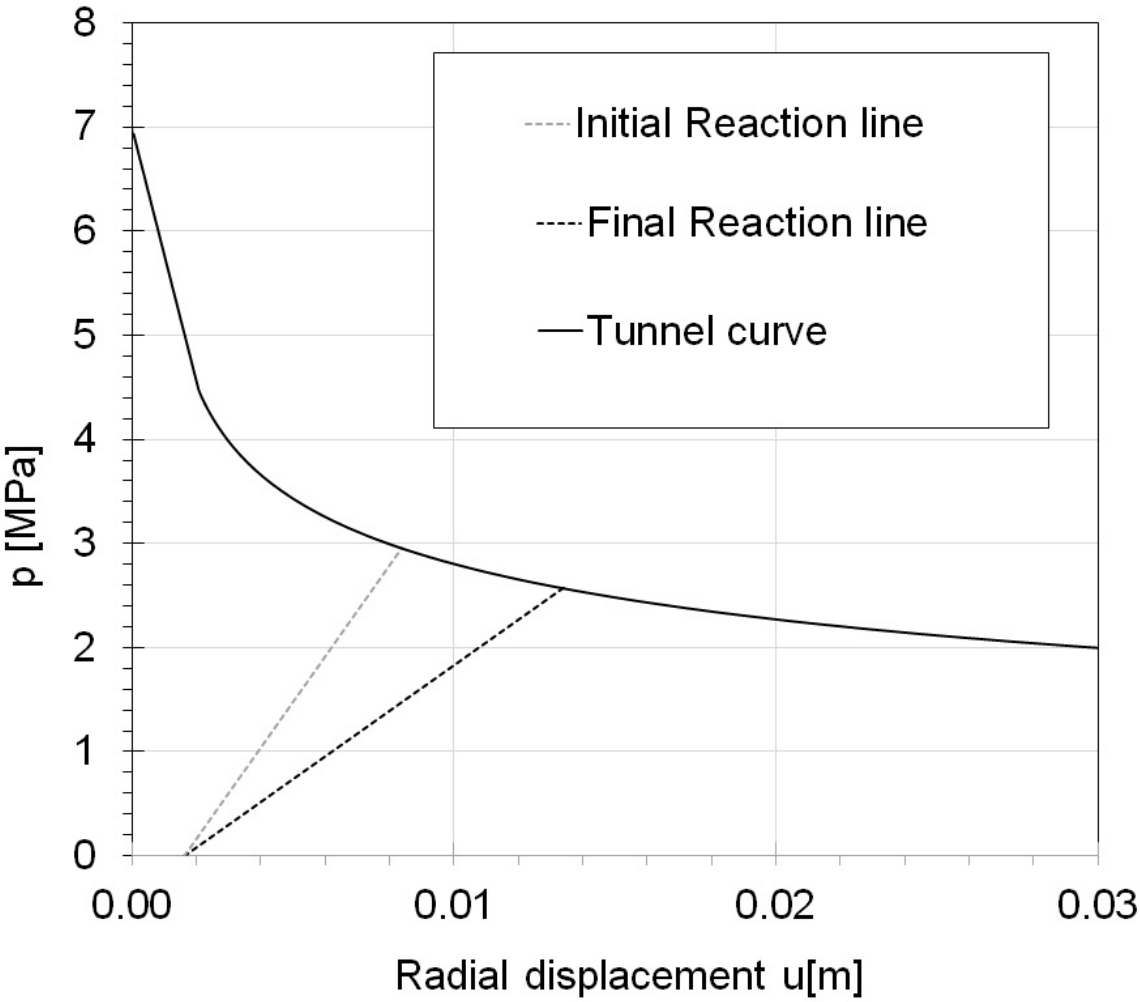

Fig. 6 Case 2: Convergence-confinement curve of the tunnel and the initial and final reaction line of the shotcrete lining.

Changing the value of E_∞ will also change the value of E_2, which, as seen previously, depends on E_1 and E_∞. Therefore, $E_2 = E_1 = 8000\ MPa$.

The trend of the rotation changes with respect to the previous case, but in this case also it tends to attenuate over time due to the creep. Bending moments also diminish and decrease more than normal forces. The resulting reductions, in terms of maximum in absolute value, increase, and are as follows (Fig. 7):

- rotation: 30.13%;
- bending moments: 26.68%;
- normal forces: 11.20%;

291 • shear forces: 7.2%.

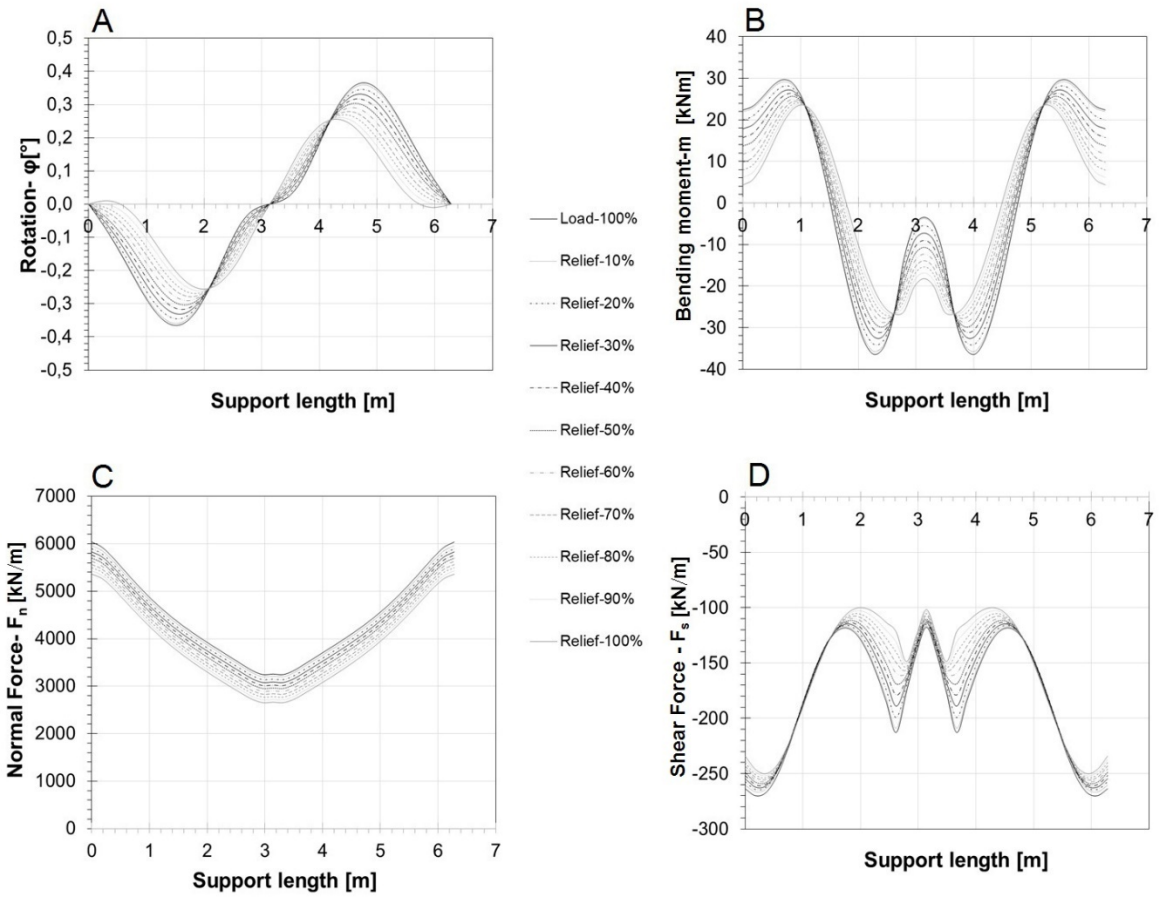

292

293 **Fig. 7 Case 2: Results of rotation (A), bending moments (B), normal (C) and shear**
294 **forces (D) for case 2 along the lining profile.**

295 As regards the variations of the elastic modulus corresponding to each step and the respec-
296 tive associated times, the results are reported in Tab. 3.

Step	E shotcrete [MPa]	t [year]
1	7638.99	0.66
2	7227.13	1.67
3	7068.87	2.18
4	6913.90	2.76
5	6762.14	3.45

6	6613.52	4.29
7	6467.98	5.37
8	6325.45	6.84
9	6185.87	9.17
10	6049.17	14.83

Tab. 3 – Case 2: variation of the elastic modulus of the SC over time during the creep process, according to the adopted mechanical scheme; time associated to each step, after the construction phase (initial condition).

Case 3

In case 3 the same parameters adopted in case 1 are used, but a different type of rock mass with better mechanical characteristics is assumed, i.e. with RMR = 60. The geomechanical parameters of the rock mass are illustrated in Tab. 4.

Rock parameter	**Unity of measure**	**Value**
Elastic modulus (E_{rm})	[MPa]	17780
Coefficient of Poisson (v)	[-]	0.30
Peak cohesion (c_p)	[MPa]	2
Residual cohesion (c_r)	[MPa]	2
Peak friction angle (φ_p)	[°]	37
Residual friction angle (φ_r)	[°]	37
Dilatancy (ψ)	[°]	16

Tab. 4 Geomechanical parameters arbitrary assumed for the rock with RMR=60.

A new convergence-confinement curve will be obtained, which will show considerably reduced displacements of the tunnel wall for the best rock mass quality (Fig. 8).

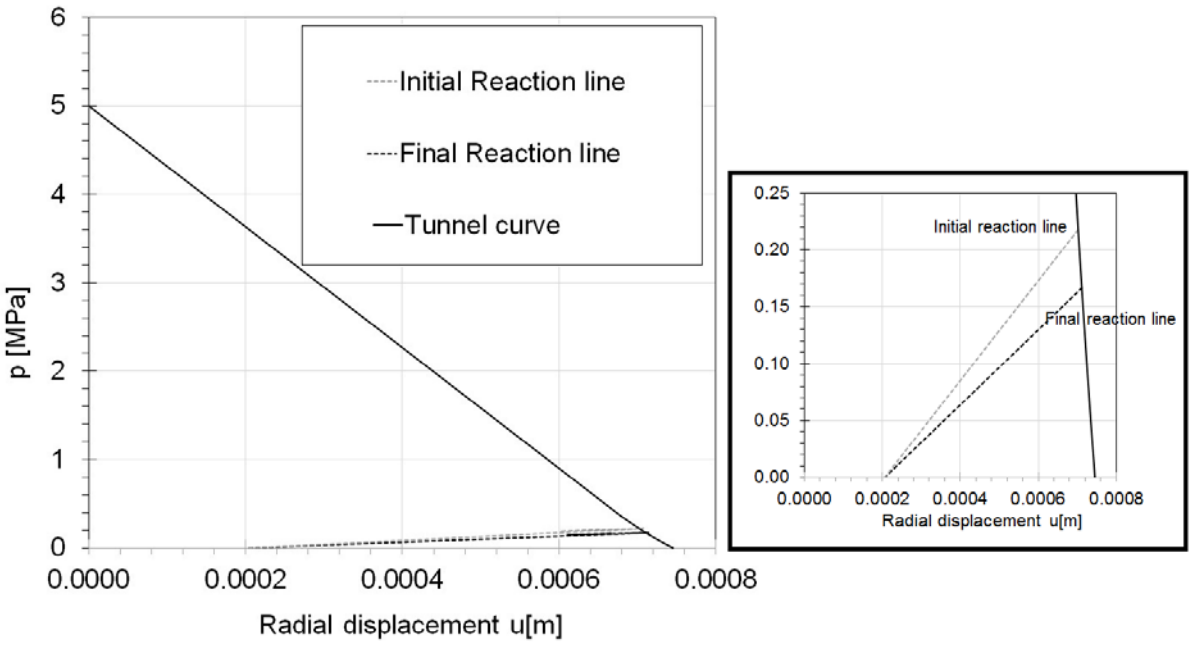

Fig. 8 Case 3: Convergence-confinement curve of the tunnel and the initial and final reaction line of the shotcrete lining (with enlargement on the right side).

The variations in the stress-strain state of the lining, from the initial condition to the final condition, are shown in Fig. 9.

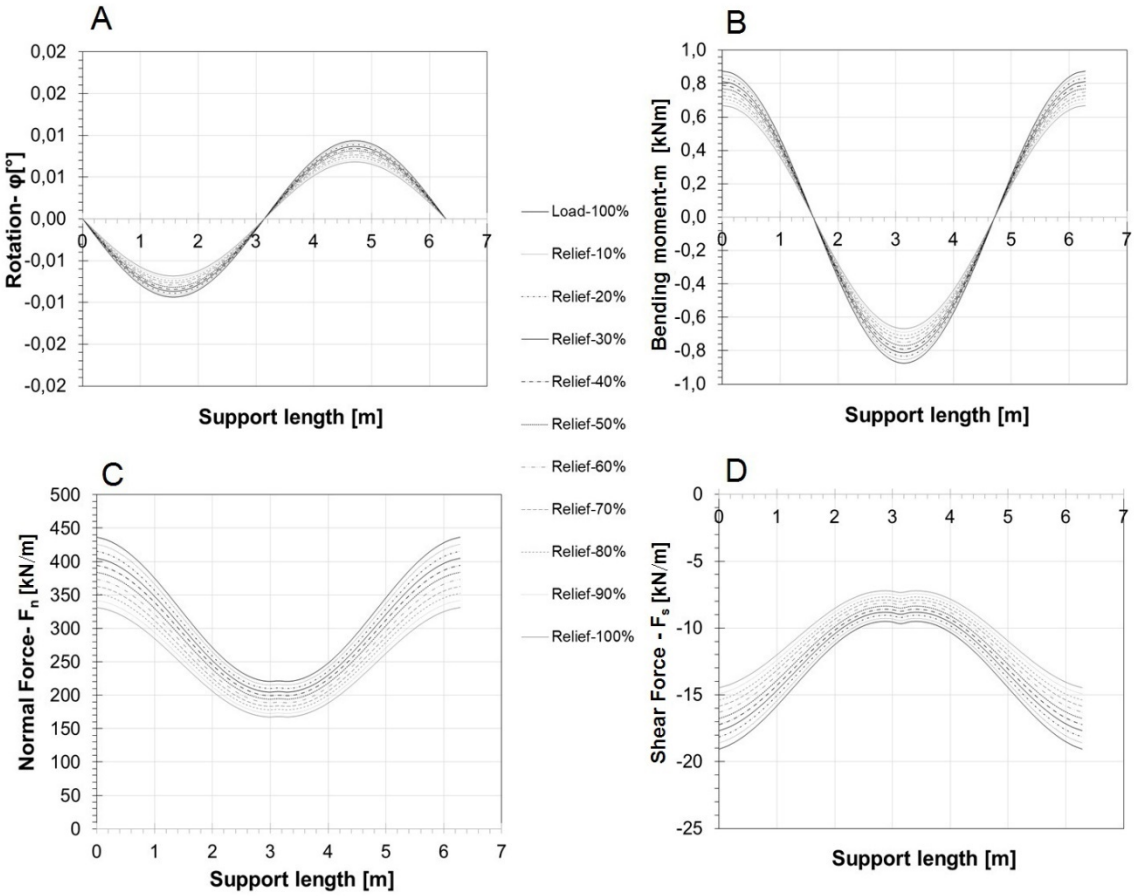

312

313 **Fig. 9 Case 3: Results of rotation (A), bending moments (B), normal (C) and shear**
314 **forces (D) for case 3 along the lining profile.**

315 The rotation changes course; however, it tends to decrease over time due to creep. Bending
316 moments also diminish and there is a greater attenuation of normal forces and shear forces
317 for this case. The resulting percentage reductions, in terms of maximum in absolute value,
318 are the following:

319 • rotation: 27.66%;
320 • bending moments: 23.34%;
321 • normal forces: 24.08%;
322 • shear forces: 24.08%.

323 As regards the variations of the elastic modulus corresponding to each step and the respec-
324 tive associated times, the results are reported in Tab. 5.

Step	E shotcrete [MPa]	t [year]
1	7474.58	0.32
2	6785.17	0.85
3	6362.81	1.29
4	5965.19	1.81
5	5590.82	2.44
6	5238.32	3.24
7	4906.40	4.31
8	4593.85	5.85
9	4299.54	8.53
10	6049.17	19.46

Tab. 5 - Case 3: variation of the elastic modulus of the SC over time during the creep process, according to the adopted mechanical scheme; time associated to each step, after the construction phase (initial condition).

Fig. 10 shows the trends in the variation of the elastic modulus of concrete over time for the 3 proposed cases as well as for other two cases:

- case 4 has a different viscosity while for E_∞ it is assumed again that it is equal to $75\%\ E_1$. Viscosity for case 4 is:

$$\eta = \frac{-3 \cdot E_2}{\ln(\frac{1}{3})} \quad (16)$$

The characteristic curve and the graphs related to the variations of rotation, normal and shear nodal displacements, bending moments, normal and shear forces are the same as in case 1. The only difference with respect to case 1 is regarding the times associated with each step and, therefore, in the development rate of secondary deformations during the creep phase.

- case 5 has an elastic modulus $E_\infty = 50\% \cdot E_1$ and a viscosity based on the assumption that the secondary deformation is equal to one third of the total secondary deformation after three years; in this case the two changes made in cases 2 and 4 are combined. The results obtained will coincide with case 2 as regards the convergence-confinement curve and the graphs related to rotation variations, bending moments, normal and shear forces, while the times associated to each step and with the module decreasing will change again (not shown).

The curves of the cases 1, 2, 4 and 5 are linked by the same E_∞ but have different viscosities and the pattern changes.

The curves characterized by the lower viscosity (case 2 and 5) and therefore by a faster creep show a trend of the elastic modulus which decreases more rapidly and each step is reached in a shorter time. The lines are obtained considering for each case 10 steps to simulate the creep process.

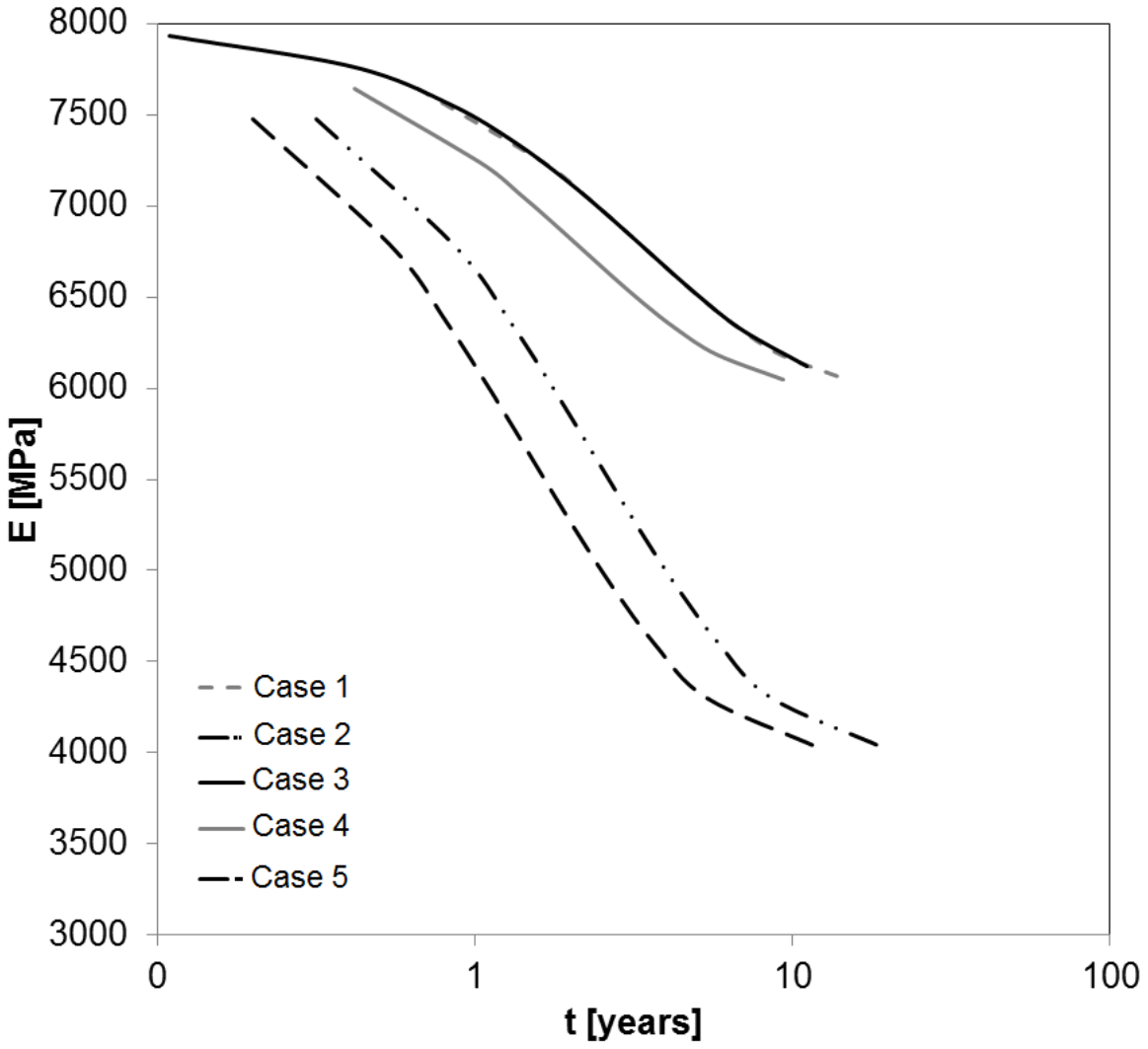

Fig. 10 Variation over the time of the elastic modulus E of the SC for the proposed cases.

Tab. 6 summarizes the results obtained in the numerical examples in terms of rotation, bending moment, normal and shear forces, in the initial and final conditions.

Rotation [°]	Max		Min	
	Initial value	Final value	Initial value	Final value
Case 1	0.365	0.320	-0.365	-0.320
Case 2	0.365	0.255	-0.365	-0.255

Case 3	0.0094	0.0068	-0.0094	-0.0068
Case 4	0.365	0.320	-0.365	-0.320
Case 5	0.365	0.255	-0.365	-0.255
Internal bending moments [kN·m]	**Initial value**	**Final value**	**Initial value**	**Final value**
Case 1	29.68	26.49	-36.43	-31.03
Case 2	29.68	23.55	-36.43	-26.71
Case 3	0.874	0.67	-0.874	-0.67
Case 4	29.68	26.49	-36.43	-31.03
Case 5	29.68	23.55	-36.43	-26.71
Internal normal forces [kN/m]	**Initial value**	**Final value**	**Initial value**	**Final value**
Case 1	6037.40	5805.82	3243.93	3034.33
Case 2	6037.40	5360.80	3243.93	2651.96
Case 3	436.46	331.35	220.64	167.51
Case 4	6037.40	5805.82	3243.93	3034.33
Case 5	6037.40	5360.80	3243.93	2651.96
Internal shear forces [kN/m]	**Initial value**	**Final value**	**Initial value**	**Final value**
Case 1	-117.67	-112.80	-269.88	-262.10
Case 2	-117.67	-100.60	-269.88	-250.21
Case 3	-9.51	-7.22	-19.06	-14.47
Case 4	-117.67	-112.80	-269.88	-262.10

Case 5	-117.67	-100.60	-269.88	-250.21

Tab. 6 Variation of the maximum and minimum values for rotation, bending moments, normal and shear forces in the initial and final conditions.

From the analysis of the results obtained, it is possible to see how the creep phenomenon on the SC used as a tunnel support produces a reduction of the bending moments, normal and shear forces over time. This phenomenon is generally more evident on bending moments, compared to normal and shear forces. When secondary deformations are important, i.e. when the creep is very evident, a more pronounced reduction of the normal and shear forces is also noted. In rock masses of good geomechanical qualities, the reduction of normal and shear forces are in percentage comparable with the reduction observed for bending moments.

These considerations turn out to be useful in the design phase of the support structure. In fact, when it is necessary to ensure the achievement of long-term lining safety factors, it is possible to take into account the creep phenomenon of the SC. This phenomenon, producing a decrease in the stress state of tunnel linings, makes it possible to increase the safety factor over time, until the final asymptotic value relative to the final situation is reached.

Conclusions

The combined analysis HRM-CCM allowed to analyze the behavior of the SC linings in the tunnel, obtaining information on the moments, normal and shear forces. The secondary deformation effects over time due to creep were taken into account in this paper, using the Voigt-Kelvin model. A new procedure has been developed, which is able to analyze the stress and strain state of a SC lining during the creep phase, considering the reduction of the loads applied to the support and the increase in the deformation of the SC over time. The analysis carried out showed that in the studied rock masses the creep has beneficial effects on the SC lining with a reduction of the stress state; in particular, in the case of the rock mass with good geomechanical quality the reduction in percentage of the normal and shear

forces is substantial and comparable to the bending moment reduction. This is not the case for the rock mass with lower geomechanical quality, for which the shear and normal forces in the lining show a negligible reduction due to the creep phenomenon, while the bending moment still remains to an high level.

References

Akroyd TNW (1962) Concrete, Properties and Manufacture. Pergamon Press.

Barla G (2001) Tunnelling under squeezing rock conditions. Eurosummer-School in Tunnel Mechanics, Innsbruck, 169-268.

Barla G (2011) Contributions to the understanding of time dependent behaviour in deep tunnels. Geomechanics and Tunnelling 4(3): 255-264, https://doi.org/10.1002/geot.201100021.

Cervera M, Oliver J, Prato T (1999) Thermo-chemo-mechanical model for concrete. II: damage and creep. Journal of Engineering Mechanics ASCE 125(9): 1028-1039, https://doi.org/10.1061/(ASCE)0733-9399(1999)125:9(1028).

Deere DU, Peck RB, Parker HW, Monsees, JE, Schmidt B (1970) Design of tunnel support systems. 49th Annual Meeting of the Highway Research Board, 12-16 January 1970, Washington D.C., United States, Highway Research Board, 26-33.

Ding Y (1998) Technologische Eigenschaften von jungen Stahlfaserbeton und Stahlfaserspritzbeton. PhD thesis, University of Innsbruck (Austria).

Do, N.A., Dias, D., Oreste, P., and Djeran-Maigre, I (2014) The behavior of the segmental tunnel lining studied by the hyperstatic reaction method. European Journal of Environmental and Civil Engineering 18(4), 489–510.

Dusseault MB, Fordham CJ (1993) Time-dependent behavior of rocks. In Hudson JA, ed. *Comprehensive Rock Engineering*. Pergamon Press 119–149.

Goodman R (1980) Introduction to Rock Mechanics, New York (US): Wiley.

405 Hellmich C, Mang HA (1999) Influence of the dilation of soil and shotcrete on the load bear-
406 ing behaviour of NATM-Tunnels. Felsbau 17:35-43.

407 Hellmilch C, Sercombe J, Ulm FJ, Mang H (2000) Modeling of early age creep of shotcrete.
408 II: application to tunneling. Journal of Engineering Mechanics ASCE 126(3):292-299,
409 https://doi.org/10.1061/(ASCE)0733-9399(2000)126:3(292).

410 Huber HG (1991) Untersuchung zum Verformungsverhalten von jungem Spritzbeton im Tun-
411 nelbau. Master thesis, University of Innsbruck (Austria).

412 Jaeger JC, Cook NGW (1979) Fundamentals of Rock Mechanics. London: Chapman and
413 Hall.

414 Kuwajima FM (1999) Early age properties of the shotcrete. In Celestino T, Parker, H, eds.
415 Shotcrete for Underground, Sao Paulo, Brazil, 153‑173.

416 MacKay J, Trottier JF (2004) Post-crack creep behaviour of steel and synthetic FRC under
417 flexural loading. In Bernard ES, ed. Shotcrete: More Engineering Developments. London:
418 Taylor & Francis, 183-192.

419 Moghadam SN, Mirzabozorg H, Noorzad A (2013) Modeling time-dependent behavior of gas
420 caverns in rock salt considering creep, dilatancy and failure. Tunnelling and Underground
421 Space Technology 33:171-185, DOI: 10.1016/j.tust.2012.10.001.

422 Melbye T (1994) Sprayed Concrete for Rock Support. Switzerland: MBT Underground Con-
423 struction Group.

424 Neville AM, Dilger WH, Brooks JJ (1983) Creep of plain and structural concrete, Harlow:
425 Construction Press.

426 Neville AM (1995) Properties of Concrete. Harlow: Addison Weslex Longman Ltd.

427 Oreste P (2007) A numerical approach to the hyperstatic reaction method for the dimension-
428 ing of tunnel supports. Tunnelling and Underground Space Technology 22(2):185–205,
429 *https://doi.org/10.1016/j.tust.2006.05.002*.

430 Oreste P (2009) The Convergence-Confinement Method: Roles and limits in modern geome-
431 chanical tunnel design. American Journal of Applied Sciences 6(4):757-771.

432 Oreste P (20015) Analysis of the Interaction between the Lining of a TBM Tunnel and the
433 Ground Using the Convergence-Confinement Method. American Journal of Applied Sciences
434 12(4):276-283. DOI: 10.3844/ajassp.2015.276.283.

435 Oreste P, Spagnoli G, Luna Ramos CA, Sebille L (2018) The Hyperstatic Reaction Method
436 for the Analysis of the Sprayed Concrete Linings Behavior in Tunneling. Geotechnical and
437 Geological Engineering, 36(4): 2143–2169, https://doi.org/10.1007/s10706-018-0454-6.

438 Rokahr RB, Lux KH (1987) Einfluss des rheologischen Verhaltens des Spritzbetons auf den
439 Ausbauwiderstand. Felsbau 5:11-18.

440 Schädlich B, Schweiger HF (2014) A new constitutive model for shotcrete. In Hicks MA,
441 Brinkgreve RBJ, Rohe A, eds. Numerical Methods in Geotechnical Engineering. Boca Raton:
442 CRC Press, 103-108.

443 Schröpfer T (1995) Numerischer Analyse des Tragverhaltens von Gebirgsstrecken mit
444 Spritzbetonausbau im Ruhrkarbon. PhD thesis, Clausthal University of Technology (Germa-
445 ny).

446 Spagnoli G, Oreste P, Lo Bianco L. (2016). New equations for estimating radial loads on
447 deep shaft linings in weak rocks. International Journal of Geomechanics 16(6): 06016006,
448 DOI: *10.1061/(ASCE)GM.1943-5622.0000657*.

449 Spagnoli G, Oreste P, Lo Bianco L. (2017) Estimation of shaft radial displacement beyond
450 the excavation bottom before installation of permanent lining in nondilatant weak rocks with a

451 novel formulation. International Journal of Geomechanics, 17(9): 04017051
452 https://doi.org/10.1061/(ASCE)GM.1943-5622.0000949.

453 Thomas A (2009) Sprayed Concrete Lined Tunnels. Oxon: Taylor and Francis.

454 Yin J (1996) Untersuchungen zum zeitabhängigen Tragverhalten von tiefliegenden Hohlrau-
455 men im Fels mit Spritzbeton. PhD thesis, Clausthal University of Technology (Germany).

456 Yu CW (1998) Creep characteristics of soft rock and modelling of creep in tunnel : determi-
457 nation of creep characteristics of soft rock and development of non-linear creep analysis
458 code for squeezing tunnel problem. PhD thesis, University of Bradford (UK).

459

460 **FIGURE CAPTION**

461 **Fig. 1 Simplified load-deformation diagram at the end of the excavation and loading**
462 **phase of the SC lining. Keys: OA represents the deformation occurring before the lin-**
463 **ing is installed. AA' represents the loads in an incompressible support; OB represents**
464 **the deformation of the walls of the tunnel; AB represents the deformation of the lining;**
465 **BB' represents the load in the support (modified after Deere et al., 1970).**

466 **Fig. 2 Evaluation of the initial and final load on the lining through the convergence-**
467 **confinement method. Key: *p* internal pressure of the tunnel; *u* radial displacement of**
468 **the tunnel wall; k_{in} and k_{fin} initial and final stifness of the SC lining; p_{in} and p_{fin} initial**
469 **and final load on the SC lining; CCC convergence-confinment curve.**

470 **Fig. 3 Voigt-Kelvin creep model (σ is the applied load, E is the elastic modulus and η is**
471 **the viscosity coefficient, ε is the deformation.**

472 **Fig. 4 Case 1: Convergence-confinement curve of the tunnel and the initial and final**
473 **reaction line of the shotcrete lining.**

474 **Fig. 5 Case 1: Results of rotation (A), bending moments (B), normal (C) and shear**
475 **forces (D) for case 1 along the lining profile.**

476 **Fig. 6 Case 2: Convergence-confinement curve of the tunnel and the initial and final**
477 **reaction line of the shotcrete lining.**

478 **Fig. 7 Case 2: Results of rotation (A), bending moments (B), normal (C) and shear**
479 **forces (D) for case 2 along the lining profile.**

480 **Fig. 8 Case 3: Convergence-confinement curve of the tunnel and the initial and final**
481 **reaction line of the shotcrete lining (with enlargement on the right side).**

482 **Fig. 9 Case 3: Results of rotation (A), bending moments (B), normal (C) and shear**
483 **forces (D) for case 3 along the lining profile.**

Fig. 10 Variation over the time of the elastic modulus E of the SC for the proposed cases.

TABLE CAPTION

Tab. 1 Geomechanical parameters arbitrary assumed for the rock with RMR=30.

Tab. 2 – Case 1: variation of the elastic modulus of the SC over time during the creep process, according to the adopted mechanical scheme; time associated to each step, after the construction phase (initial condition).

Tab. 3 – Case 2: variation of the elastic modulus of the SC over time during the creep process, according to the adopted mechanical scheme; time associated to each step, after the construction phase (initial condition).

Tab. 4 Geomechanical parameters arbitrary assumed for the rock with RMR=60.

Tab. 5 - Case 3: variation of the elastic modulus of the SC over time during the creep process, according to the adopted mechanical scheme; time associated to each step, after the construction phase (initial condition).

Tab. 6 Variation of the maximum and minimum values for rotation, bending moments, normal and shear forces in the initial and final conditions.